INFORMATICA, 2014, Vol. 25, No. 1, 113–137

JND-Based Watermark Embedding and GA-Based Watermark Extraction with Fuzzy Inference System for Image Verification

Hung-Hsu TSAI[1], Shih-Che LO[2]*

[1]*Department of Information Management, National Formosa University*
Huwei, Yunlin 632, Taiwan
[2]*Department of Industrial Management, National Taiwan University of Science and Technology*
Taipei 106, Taiwan
e-mail: thh@nfu.edu.tw, sclo@mail.ntust.edu.tw

Received: May 2011; accepted: September 2013

Abstract. This paper presents an adaptive image-watermarking technique based on just-noticeable distortion (JND) profile and fuzzy inference system (FIS) optimized with genetic algorithm (GA). Here it is referred to as the AIWJFG technique. During watermark embedding, it embeds a watermark into an image by referring the JND profile of the image so as to make the watermark more imperceptible. It employs image features and local statistics in the construction of an FIS, and then exploits the FIS to extract watermarks without original images. In addition, the FIS can be further optimized by a GA to improve its watermark-extraction performance remarkably. Experimental results demonstrate that the AIWJFG technique not only makes the embedded watermarks further imperceptible but also possesses adaptive and robust capabilities to resist on image-manipulation attacks being considered in the paper.

Key words: data hiding, genetic algorithms, image verification, image watermarking, just-noticeable distortion, fuzzy inference system, fuzzy logic.

1. Introduction

Due to the rapid development of digital technologies, various formats of multimedia, such as audio, images, and video, are readily copied or exchanged through the Internet without any limits. Consequently, the copyright protection of multimedia becomes a new important problem in wide-range applications for the Internet, for example, e-commerce (Mukherjee *et al*., 2004). Digital watermarking is an effective way of solving the problem. Many image-watermarking techniques have been proposed and have gained prominent results to diminish the unauthorized proliferation of multimedia greatly (Moon *et al*., 2007).

In general, the image-watermarking schemes can be developed in either the spatial or frequency domain. First, the schemes are accomplished in the frequency domain (Barni *et al*., 2001; Paquet *et al*., 2003; Wang and Pearmain, 2004; Zhao *et al*.,

*Corresponding author.

2004). Their embedding process is to make a small modifications to the coeffcients which are obtained through an appropriate transformation, such as Discrete Cosine Transform (DCT) (Hsu and Wu, 1999; Wang and Pearmain, 2004) or Discrete Wavelet Transform (DWT) (Joo *et al*., 2002; Tsai and Liu, 2008; Tsai and Wang, 2008). The other class of watermarking schemes is designed in the spatial domain (Mukherjee *et al*., 2004; Tsai and Sun, 2007; Yu *et al*., 2001). Their computational complexity is less than that of the schemes developed in the frequency domain. The latter schemes require more computational time in data transformation than the former schemes. Moreover, while encountering the image-processing attacks devised in the frequency domain, the robustness of the schemes developed in frequency domain is generally better than that of the schemes developed in spatial domain. Despite this, the spatial information of images should be employed in the design of watermarking schemes for enhancing their robustness in resisting the attacks which are performed in the spatial domain, such as blurring, cropping, painting, scaling, and histogram equalization. Subsequently, some techniques have been developed in both spatial and frequency domains, which simultaneously take the advantages of the schemes of these two categories stated above (Shih and Wu, 2003; Yu *et al*., 2003).

Even though the above watermarking techniques have well performed in the copyright protection of images, some techniques still inherit the following drawbacks. First, some of them require the original image during watermarking detection or extraction (Joo *et al*., 2002; Shih and Wu, 2003). Consequently, these techniques cannot solve the deadlock problem, introducing the ambiguity of the ownership of images. Second, some of proposed methods merely performed the watermark detection instead of the watermark extraction (Barni *et al*., 2001). Specifically, these methods fail in getting tracing clues regarding piracy evidence. Although several image-watermarking techniques, such as the methods of Paquet *et al*. (2003) and Zhao *et al*. (2004), have been proposed to overcome the above two drawbacks, these techniques did not utilize the image features in the spatial domain to enhance the immunization against the attacks developed in spatial domain. Accordingly, the AIWJFG technique is developed to improve the performance of the proposed techniques having these three drawbacks.

Several methods, which are based on fuzzy theory, have been developed for image watermarking (Chang *et al*., 2005; Hsieh and Tseng, 2005; Lou and Yin, 2002). In the methods of Lou and Yin (2002) and Hsieh and Tseng (2005), an FIS is used in the design of their watermark embedding algorithms. In the method of Chang *et al*. (2005), a fuzzy-classification approach is also exploited to develop a watermark insertion algorithm. In contrast, an FIS is employed for the watermark extraction of the AIWJFG technique. A goal of devising the AIWJFG technique is to enhance the transparency and robustness of the traditional techniques. During watermark embedding, the AIWJFG technique adaptively modifies target pixels by considering the image features of the target pixels and also referring their associated JND profile values. During watermark extraction, the AIWJFG technique integrates the image features and local statistics to create an FIS which contains three fuzzy input variables, 14 fuzzy inference rules, and a single fuzzy output variable. The AIWJFG technique employs the FIS to estimate the watermark. In addition,

the FIS is optimized by using a GA to further increase the correct rate of watermark estimates. Here the AIWJFG technique extracts the watermarks without the information of original images, because it applies the FIS to extract watermarks. Observing experimental results, the AIWJFG technique not only makes watermarks more imperceptible but also definitively has both adaptive and robust abilities in the resistance to image-processing manipulations or attacks under consideration.

The rest of the paper is organized as follows. Section 2 introduces the JND profile for an image, image features, local statistics, and an FIS. Section 3 then describes the watermark-embedding and watermark-extraction algorithms of the AIWJFG technique, and states the FIS which is further optimized by using a GA. Subsequently, Section 4 shows experimental results. Finally, Section 5 gives conclusions.

2. Background

2.1. *Image and Watermark Representations*

Let $X = [x_{ij}]_{M\times N}$ denote a gray-level image with size $M \times N$ where $x_{ij} \in \{0, 1, \ldots, 255\}$ represents a gray level of the pixel at position (i, j) on X. The image X can be partitioned into a set S of blocks with size 3×3 where $S = \{X_{ij}\}$. Each block X_{ij} with the center pixel x_{ij} can be expressed as a form

$$X_{ij} = \begin{bmatrix} x_{i-1,j-1} & x_{i-1,j} & x_{i-1,j+1} \\ x_{i,j-1} & x_{i,j} & x_{i,j+1} \\ x_{i+1,j-1} & x_{i+1,j} & x_{i+1,j+1} \end{bmatrix}. \tag{1}$$

A stamp binary image with size $m \times n$ is taken as the watermark W. Using the row-major method, the watermark W can be denoted by $W = (w_1, w_2, \ldots, w_{m\times n})$, where $w \in \{0, 1\}$, $k = 1, 2, \ldots, m \times n$. Similarly, the extracted watermark $\hat{W}$ is expressed by $\hat{W} = (\hat{w}_1, \hat{w}_2, \ldots, \hat{w}_{m\times n})$, where $\hat{w} \in \{0, 1\}$, $k = 1, 2, \ldots, m \times n$.

2.2. *JND Profile Calculation*

The psycho-visual properties of the HVS have been effectively applied in image processing (Jain, 1989). The JND is a key concept of the HVS for integrating all of human visual properties (Chou and Li, 1995; Delaigle *et al*., 1998). A JND threshold represents a minimum distortion or limit. If the change to each pixel of an image is below the limit, the difference between the original image and its changed version is without making perceptible alteration to image-visual quality. That is, the change in a pixel value is imperceptible generally if the distortion magnitude of the pixel value is under the limit specified by its corresponding JND threshold. A JND profile of an original image represents a 2-D threshold of the error visibility, below which reconstruction errors are rendered imperceptible. Experimental results show that there are two important factors that dominate the error visibility threshold at each pixel. These two factors are background intensity and spatial nonuniformity (Chou and Li, 1995). Chou's method takes the above two factors into ac-

count while computing the JND profile. A JND profile for pixel (i, j) is computed by

$$\begin{aligned}
&JND(i,j) = \max\left\{f_1\big(bg(i,j), mg(i,j)\big),\, f_2\big(bg(i,j)\big)\right\},\\
&f_1\big(bg(i,j), mg(i,j)\big) = mg(i,j)\alpha\big(bg(i,j)\big) + \beta\big(bg(i,j)\big),\\
&f_2\big(bg(i,j)\big) = \begin{cases} T_0\left(1 - \left(\frac{bg(i,j)}{127}\right)^{\frac{1}{2}}\right) + 3, & \text{for } bg(i,j) \leqslant 127,\\ \gamma\big(bg(i,j) - 127\big) + 3, & \text{for } bg(i,j) > 127, \end{cases}\\
&\alpha\big(bg(i,j)\big) = 0.0001bg(i,j) + 0.115,\\
&\beta\big(bg(i,j)\big) = \lambda - 0.01bg(i,j),
\end{aligned} \tag{2}$$

where T_0, γ, and λ are 17, 3/128, and 1/2, respectively. In addition, f_1 denotes the background intensity, f_2 represents the spatial nonuniformity, $mg(i, j)$ stands for the maximum weighted average of luminance differences around the pixel at (i, j), and $bg(i, j)$ expresses the average background luminance of luminance differences around the pixel at (i, j). Here α and β are the background-luminance dependent functions that specify the slope of the line and the intersection with the visibility threshold axis. During watermark embedding, the AIWJFG technique considers image features of target pixels to be embedded and also refers their corresponding JND profile values to achieve adaptive changes to the pixels.

2.3. *Image Features and Local Image Statistics*

The AIWJFG technique creates three input variables, G, U, and V, and then constructs 14 fuzzy rules constituting a rulebase in the FIS to be used for watermark retrievals. The first variable G is to measure the possibility that the center pixel x_{ij} in the block X_{ij} is on a smooth image feature. Here the smooth image feature is performed by using an estimated standard deviation of the absolute differences among the center pixel x_{ij} and its neighboring pixels in X_{ij} (Umbaugh, 1998). Specifically, an estimated standard deviation G_{ij} for x_{ij} can be formularized as

$$G_{ij} = \left[\frac{1}{(2l_G+1)\times(2k_G+1)-1}\sum_{l=-l_G}^{l_G}\sum_{k=-k_G}^{k_G}\big(|x_{i+l,j+k} - x_{ij}| - m_{ij,G}\big)^2\right]^{\frac{1}{2}} \tag{3}$$

where the size of the block X_{ij} equals $l_G \times k_G$, and $m_{ij,G}$ is defined by

$$m_{ij,G} = \frac{1}{(2l_G+1)\times(2k_G+1)-1}\left(\sum_{l=-l_G}^{l_G}\sum_{k=-k_G}^{k_G}|x_{i+l,j+k} - x_{ij}|\right).$$

In general, low G_{ij} indicates a high possibility that the center pixel x_{ij} is located in a smooth image feature.

Two local image statistics, $m_{ij,U}$ and $m_{ij,V}$, which are calculated in the spatial domain, are taken as two inputs of the fuzzy rules in an FIS for two variables U and V, respectively. The first one $m_{ij,U}$ denotes the average of all pixel values in an image block X_{ij} excluding

the center pixel value. The other $m_{ij,V}$ is the average of two pixel values in the block X_{ij} where these two pixel values are closest to the center pixel x_{ij}. For an image block X_{ij}, $m_{ij,U}$ and $m_{ij,V}$ can be, respectively, defined by

$$m_{ij,U} = \frac{1}{(2l_U + 1) \times (2k_U + 1) - 1}\left[\left(\sum_{l=-l_U}^{l_U}\sum_{k=-k_U}^{k_U} |x_{i+l,j+k}|\right) - x_{ij}\right] \tag{4}$$

and

$$m_{ij,V} = \frac{1}{2}\left(s_{ij}^1 + s_{ij}^2\right) \tag{5}$$

where s_{ij}^1 and s_{ij}^2 are two pixel values which are closest to the center pixel x_{ij}. Additionally, the size of the block X_{ij} equals $l_U \times k_U$. Note that the size of the block X_{ij} used for the computations of $m_{ij,U}$ and $m_{ij,V}$ is smaller than that of X_{ij} used for the computation of G_{ij}. In the experiment of the paper, l_G and k_G are set to 2, but, meanwhile, l_U and k_U are set to 1.

Accordingly, for an image block X_{ij}, (G_{ij}, U_{ij}, V_{ij}) represents an input vector of the FIS where

$$U_{ij} = x_{ij} - m_{ij,U} \tag{6}$$

and

$$V_{ij} = x_{ij} - m_{ij,V}. \tag{7}$$

2.4. *Fuzzy Inference System*

Fuzzy logic is a convenient approach for modeling the human knowledge, and also is an effective way for realizing the conceptual design of an intelligent system (Ross, 2004; Wang, 1997). So far, diverse applications of fuzzy logic have been growing rapidly (Arakawa, 1996; Own *et al.*, 2006). In the paper, an FIS based on fuzzy logic is applied in the watermark extraction. Figure 1 displays a general structure of an FIS consisting of four principle constituents, Fuzzifier, Fuzzy Rule Base, Fuzzy Inference Engine, and Defuzzifier. Fuzzifier maps a crisp input to a fuzzy degree via its corresponding fuzzy set with an appropriate membership function. Conversely, Defuzzifier maps a fuzzy set to a crisp value. Fuzzy Rule Base includes a set of fuzzy rules. Roughly speaking, each rule is represented with the format of If-then. Fuzzy Inference Engine evaluates the fuzzy degree of the premise part of each fuzzy rule, and then shapes each fuzzy set of the consequent part of each rule. Next, Fuzzy Inference Engine calculates these fuzzy sets for each rule by using t-norm or s-norm operators if the consequent part of each rule is a compound fuzzy proposition. Finally, the output of Fuzzy Inference Engine is a fuzzy set which is obtained by using an aggregation operator, such as a union operation for fuzzy sets, to aggregate entire fuzzy outputs (fuzzy sets) of fuzzy rules. Mamdani's and Sugeno's methods are two popular instances for Fuzzy Inference Engine (Ross, 2004; Wang, 1997).

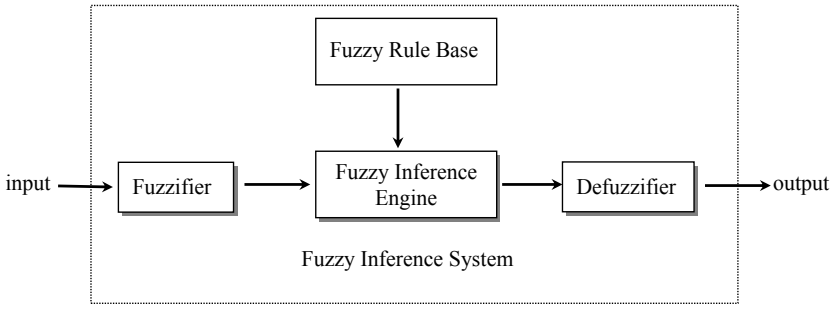

Fig. 1. A general structure of an FIS.

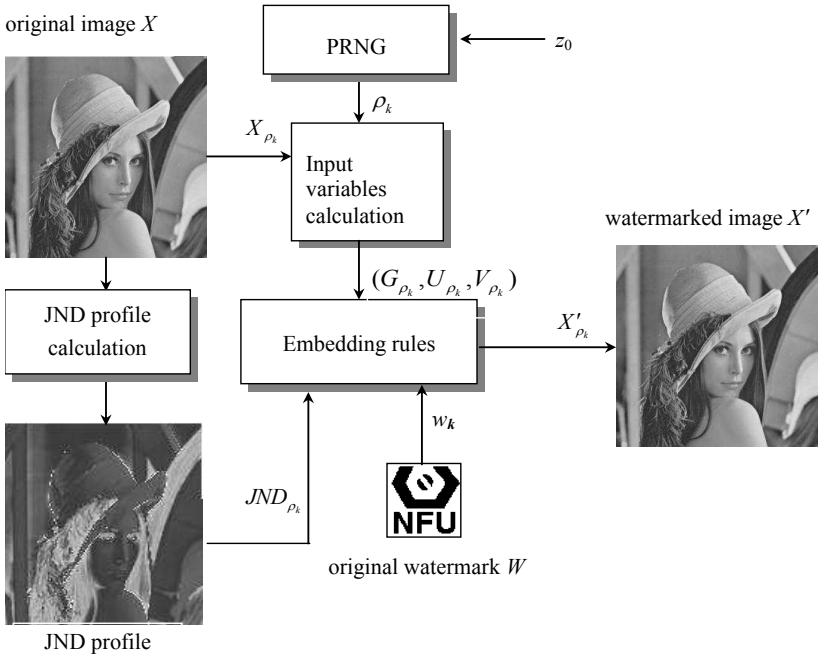

Fig. 2. The structure of the watermark embedding of the AIWJFG technique.

3. The AIWJFG Technique

3.1. *Watermark Embedding*

Figure 2 shows the structure of the watermark embedding of the AIWJFG technique. First, the component PRNG represents a pseudo-random number generator (PRNG) which generates a sequence of random positions. The length of the sequence of random positions is $m \times n$, which equals the size of the watermark W.

The algorithm of the PRNG is based on a quadratic residue generator which is proposed by Blum et al. and called the Blum-Blum-Shub generator (BBSG) (Blum *et al.*,

1986). Let z_0 be a seed used in the BBSG. Next, the BBSG generates the kth pseudo-random number computed by

$$z_k = z_k^2 - 1 \bmod R, \quad \text{for } k \leqslant 1,$$

where R is the product of two large primes that should be congruent to 3 modulus 4. Hence the BBSG serves as the PRNG securing a set of pseudorandom positions if the seed z_0 is unknown. By presenting the BBSG with a seed, z_0, and the product R of two large primes, it can randomly generate a sequence, $\boldsymbol{P}$, of positions from an image X. The sequence $\boldsymbol{P}$ can be represented as

$$\boldsymbol{P} = (\rho_1, \rho_2, \ldots, \rho_k, \ldots, \rho_{m\times n}), \tag{8}$$

where $\rho_k = (i_k, j_k)$ stands for the kth pseudo-random position on X. Hereafter the position symbol (i_k, j_k) is replaced with ρ_k in the following context.

The component, JND Profile Calculation, computes a JND profile for an image X according to (2). The information of a JND profile represents the error visibility thresholds of X. The component, Embedding Rules, denotes a method of adaptively modifying pixels via referring to the JND profile for X. That is, the method can control the modification to each pixel with appropriate strength. Specifically, the process of hiding the kth watermark bit w_k in the image block X_{ρ_k} is to alter the pixel value x_{ρ_k}. The magnitude of the alternation to the pixel depends on its corresponding JND value for X_{ρ_k}, namely JND_{ρ_k} where $JND_{\rho_k} \geqslant 0$ for each k. In Embedding Rules, the modification to x_{ρ_k} is specified by

$$x'_{\rho_k} = x_{\rho_k} + \alpha_k(2w_k - 1)JND_{\rho_k}, \tag{9}$$

where α_k controls the modification strength. In order to reduce the false estimate for watermark extraction, α_k is determined by

$$\alpha_k = \max(\alpha_{k_1}, \alpha_{k_2}) \tag{10}$$

where

$$\alpha_{k_1} = \left\lceil \frac{U_{\rho_k}}{JND_{\rho_k}} \right\rceil \quad \text{and} \quad \alpha_{k_2} = \left\lceil \frac{V_{\rho_k}}{JND_{\rho_k}} \right\rceil, \quad \text{if } w_k = 0 \tag{11}$$

and

$$\alpha_{k_1} = \left\lceil \frac{-U_{\rho_k}}{JND_{\rho_k}} \right\rceil \quad \text{and} \quad \alpha_{k_2} = \left\lceil \frac{-V_{\rho_k}}{JND_{\rho_k}} \right\rceil, \quad \text{if } w_k = 1. \tag{12}$$

Here $\lceil\cdot\rceil$ represents the ceiling function.

Let X_{ρ_k} and X'_{ρ_k} denote an original image block and its watermarked version, respectively. The algorithm for the watermark embedding of the AIWJFG technique is described as follows.

Step 1. Input an original image X. Given z_0, R, and T_α, set $k = 1$.
Step 2. Generate a sequence $\boldsymbol{P}$ of pseudo-random positions by using (8).
Step 3. Take X_{ρ_k}. Compute JND_{ρ_k}, U_{ρ_k}, V_{ρ_k}, and α_k by using (2), (6), (7), and (10)–(12), respectively.
Step 4. Embed w_k into x_{ρ_k} by modifying the pixel x_{ρ_k} with (9). Output the watermarked block X'_{ρ_k}.
Step 5. Repeat Steps 3–4 until all bits w_k, for $k = 1, \ldots, m \times n$, are embedded.
Step 6. Output the watermarked image X'. Securely keep z_0, R, m, and n.

Here the paper claims that the false estimate of w_k, for each k, can be greatly reduced while using the watermark-embedding algorithm of the AIWJFG technique during watermark extraction. The following lemma justifies the claim.

Lemma 1. *In the above watermark-embedding algorithm, each original pixel x_{ρ_k} is changed by using* (9)*. Let α_k be determined according to* (10)–(12)*, and then be applied in* (9) *to calculate x'_{ρ_k}. In the ideal case, for each k, the estimated watermark bit $\hat{w}_k$ should identify with the original watermark bit w_k. This is, each $\hat{w}_k$ is estimated correctly during watermark extraction.*

Proof. For the first case of $w_k = 1$, if x_{ρ_k} is on a smooth region, then the following result,

$$x'_{\rho_k} - m_{\rho_k,U} = x_{\rho_k} + \alpha_{k_1} JND_{\rho_k} - m_{\rho_k,U} = U_{\rho_k} + \alpha_{k_1} JND_{\rho_k} \tag{13}$$

can be obtained. To choose $\alpha_{k_1} \geqslant \lceil \frac{-U_{\rho_k}}{JND_{\rho_k}} \rceil$ yields $U_{\rho_k} + \alpha_{k_1} JND_{\rho_k} > 0$. Accordingly, (13) implies $x'_{\rho_k} - m_{\rho_k,U} > 0$. Note that $JND_{\rho_k} \geqslant 0$, for each k, according to (2). On the other hand, if x_{ρ_k} is on a non-smooth region, then we have

$$x'_{\rho_k} - m_{\rho_k,V} = x_{\rho_k} + \alpha_{k_2} JND_{\rho_k} - m_{\rho_k,V} = V_{\rho_k} + \alpha_{k_2} JND_{\rho_k}. \tag{14}$$

Subsequently, $\exists \alpha_{k_2} \geqslant \lceil \frac{-V_{\rho_k}}{JND_{\rho_k}} \rceil$ s.t. $V_{\rho_k} + \alpha_{k_2} JND_{\rho_k} > 0$. Thus, (14) implies $x'_{\rho_k} - m_{\rho_k,V} > 0$. Therefore, either x_{ρ_k} is on a smooth region or not, these two inequalities $x'_{\rho_k} - m_{\rho_k,U} > 0$ and $x'_{\rho_k} - m_{\rho_k,V} > 0$ hold while choosing $\alpha_k = \max(\alpha_{k_1}, \alpha_{k_2})$ where $\alpha_{k_1} = \lceil \frac{-U_{\rho_k}}{JND_{\rho_k}} \rceil$ and $\alpha_{k_2} = \lceil \frac{-V_{\rho_k}}{JND_{\rho_k}} \rceil$. Consequently, $\hat{w}_k$ is set to 1. For each k, the estimated watermark bit $\hat{w}_k$ equals the original watermark bit w_k.

Applying the similar way to the second case of $w_k = 0$, two inequalities $x'_{\rho_k} - m_{\rho_k,U} < 0$ and $x'_{\rho_k} - m_{\rho_k,V} > 0$ are true while choosing $\alpha_k = \max(\alpha_{k_1}, \alpha_{k_2})$ where $\alpha_{k_1} = \lceil \frac{U_{\rho_k}}{JND_{\rho_k}} \rceil$ and $\alpha_{k_2} = \lceil \frac{V_{\rho_k}}{JND_{\rho_k}} \rceil$. □

3.2. *Watermark Extraction*

Figure 3 depicts the structure of the watermark extraction of the AIWJFG technique. The component PRNG, which is the same as that used in the watermark embedding of the AIWJFG technique, generates a sequence of random positions for the watermarked

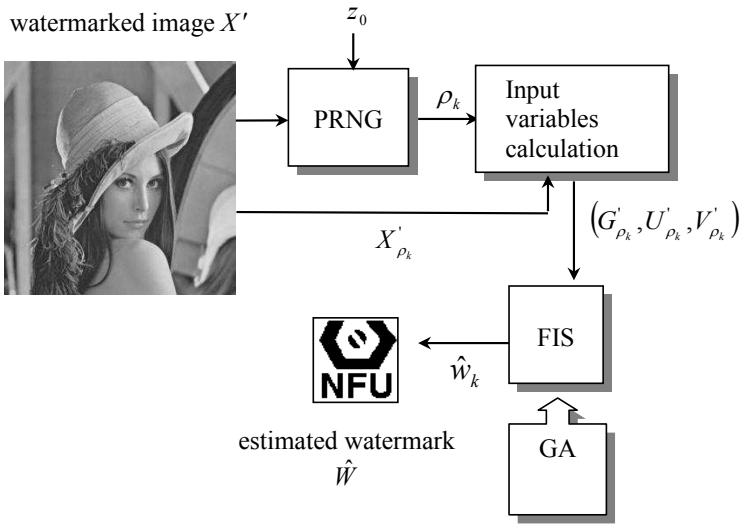

Fig. 3. The structure of the watermark extraction of the AIWJFG technique.

X'. Because of using the same seed, z_0, the sequence $\boldsymbol{P}$ is the same as that employed in the watermark-embedding procedure. The task of the watermark extraction is to estimate the values of watermark bits $\hat{w}_k$ from watermarked blocks X'_{ρ_k}, for each k. In addition, the component, Input Variables Calculation, which is the same as that exploited in the watermark-embedding procedure, computes $(G'_{\rho_k}, U'_{\rho_k}, V'_{\rho_k})$ for X'_{ρ_k} by using (3), (6), and (7). A merit of the AIWJFG technique is to utilize an FIS in the watermark extraction without original images. In order to improve the watermark-extraction performance of the AIWJFG technique, the FIS is further optimized (trained or learned) by using a GA. The algorithm for the watermark extraction of the AIWJFG technique is summarized as follows.

Step 1. Input watermarked image X'. Given z_0, R, m, and n, set $k = 1$.
Step 2. Generate a sequence $\boldsymbol{P}$ of pseudo-random positions via employing (8).
Step 3. Take X'_{ρ_k}. Compute G'_{ρ_k}, U'_{ρ_k}, and V'_{ρ_k} by using (3), (6), and (7), respectively.
Step 4. Exploit the FIS, which is trained by a GA, to estimate $\hat{w}_k$ from X'_{ρ_k}.
Step 5. Repeat Steps 3–4 until all bits $\hat{w}_k$, for $k = 1, \ldots, m \times n$, are estimated.

3.3. *Design of an FIS for Watermark Extraction*

The component FIS of the AIWJFG technique includes 14 fuzzy rules which are designed using these three fuzzy (input) variables, G, U, and V. For a watermarked image block X'_{ρ_k}, the inputs for G, U, and V are a possibility G'_{ρ_k} for x'_{ρ_k} located in a smooth image region, a difference U'_{ρ_k} between x'_{ρ_k} and $m'_{ij,U}$, and a difference V'_{ρ_k} between x'_{ρ_k} and $m'_{ij,V}$, respectively. Table 1 lists 14 fuzzy rules where $\hat{w}$ stands for the output variable of each fuzzy rule. Fuzzy linguistic atoms for G are *small, medium*, and *large*. For U and V,

Table 1
Fuzzy rules in the FIS for watermark extraction.

Rules	Fuzzy propositions
1	If G is *small* and U is *positively-large* then $\hat{w}$ is *very-positive*
2	If G is *small* and U is *positively-medium* then $\hat{w}$ is *positive*
3	If G is *small* and U is *positively-small* then $\hat{w}$ is *positive*
4	If G is *small* and U is *negatively-small* then $\hat{w}$ is *negative*
5	If G is *small* and U is *negatively-large* then $\hat{w}$ is *negative*
6	If G is *small* and U is *negatively-medium* then $\hat{w}$ is *very-negative*
7	If G is *medium* and U is *positively-medium* and V is *positively-large* then $\hat{w}$ is *very-positive*
8	If G is *medium* and U is *positively-medium* and V is *positively-medium* then $\hat{w}$ is *positive*
9	If G is *medium* and U is *negatively-medium* and V is *negatively-medium* then $\hat{w}$ is *negative*
10	If G is *medium* and U is *negatively-medium* and V is *negatively-large* then $\hat{w}$ is *very-negative*
11	If G is *large* and U is *positively-medium* and V is *positively-large* then $\hat{w}$ is *very-positive*
12	If G is *large* and U is *positively-medium* and V is *positively-medium* then $\hat{w}$ is *positive*
13	If G is *large* and U is *negatively-medium* and V is *negatively-medium* then $\hat{w}$ is *negative*
14	If G is *large* and U is *negatively-medium* and V is *negatively-large* then $\hat{w}$ is *very-negative*

Table 2
Brief descriptions to the concepts for the design of the fuzzy rules.

Rules	Human concepts
1	x'_{ρ_k} is very likely in a smooth-like region, and is very likely hidden by $w_k = 1$
2	x'_{ρ_k} is moderately likely in a smooth-like region, and is likely hidden by $w_k = 1$
3	x'_{ρ_k} is likely in a smooth-like region, and is likely hidden by $w_k = 1$
4	x'_{ρ_k} is likely in a smooth-like region, and is likely hidden by $w_k = 0$
5	x'_{ρ_k} is moderately likely in a smooth-like region, and is likely hidden by $w_k = 0$
6	x'_{ρ_k} is very likely in a smooth-like region, and is very likely hidden by $w_k = 0$
7	x'_{ρ_k} is very likely in a thin-line-like region, and is very likely hidden by $w_k = 1$
8	x'_{ρ_k} is likely in a thin-line-like region, and is likely hidden by $w_k = 1$
9	x'_{ρ_k} is likely in a thin-line-like region, and is likely hidden by $w_k = 0$
10	x'_{ρ_k} is very likely in a thin-line-like region, and is very likely hidden by $w_k = 0$
11	x'_{ρ_k} is very likely in an edge-like region, and is very likely hidden by $w_k = 1$
12	x'_{ρ_k} is likely in an edge-like region, and is likely hidden by $w_k = 1$
13	x'_{ρ_k} is likely in an edge-like region, and is likely hidden by $w_k = 0$
14	x'_{ρ_k} is very likely in an edge-like region, and is very likely hidden by $w_k = 0$

their fuzzy linguistic values include *positively-large, positively-medium, positively-small, negatively-small, negatively- medium, and negatively-large*. Fuzzy linguistic terms for $\hat{w}$ are *positive, negative, very-positive, and very-negative*.

3.4. *The Design Concepts for the Fuzzy Rules*

The design concepts of the fuzzy rules are briefly described in Table 2. The FIS includes 14 fuzzy rules which are constructed according to three principal human concepts for watermark extraction. Roughly speaking, image features of image blocks in spatial domain can be categorized into three distinct classes including the smooth-like, the thin-line-like,

and the edge-like image regions (Jain, 1989; Arakawa, 1996). The fuzzy variable G plays an important role in the design of fuzzy rules. In the first human concept, a small value for G points out a high possibility that x'_{ρ_k} locates in a smooth-like image region. Meanwhile, according to Lemma 1, the fact that U is positive (or negative) should definitely imply that a positive (or negative) value is superimposed on x_{ρ_k}. Here V can be ignored because U and V performs the same result if x_{ρ_k} is in a smooth-like image region. Regarding the first fuzzy rule, the phenomenon that U is positively large indicates that the watermarked pixel x'_{ρ_k} is likely hidden in the case of $w_k = 1$. Accordingly, the conceptual knowledge reveals that x'_{ρ_k} is very likely in the smooth-like region and has a large positive difference between x'_{ρ_k} and the average of its neighborhood pixels. Also, the design concept can be used in the converse (negative) case for the design of the 6th fuzzy rule as an estimate of the case of $w_k = 0$.

Second, a medium value for G signifies that the possibility of that x'_{ρ_k} is in a thin-line-like region is very high. At the same time, the fact that U is positive and V is positively large implies that the watermarked pixel x'_{ρ_k} is very likely hidden in the case of $w_k = 1$. The reason is that the fuzzy variable V, defined in (7), performs the thin-line detection. The conceptual knowledge is applied to create the 7th fuzzy rule. The analogous concept can be exploited in the converse case for the design of the 10th rule as an estimate of the case of $w_k = 0$.

Finally, a large value for G implies that the possibility of that x'_{ρ_k} is on an edge-like image region is very high. The fact that U is positive and V is positively large indicates a high possibility of that the watermarked pixel x'_{ρ_k} is very likely hidden in the case of $w_k = 1$. For the opposite case, the fact that U is negative and V is negatively large conveys that the watermarked pixel x'_{ρ_k} is very likely hidden in the case of $w_k = 0$. Consequently, these two design concepts can be applied to devise the 11th and 14th rules. Next, an evidence that both U and V are positive or negative reveals that the watermarked pixel x'_{ρ_k} is likely hidden in the case of $w_k = 1$ or 0, respectively. These two design concepts are utilized in the design of the 12th and the 13th rules.

3.5. *Membership Functions of the FIS*

Bell-shape-like functions are exploited to realize the membership functions of these linguistic values of the FIS. The membership functions, defined by (15), are used for representing *small*, *negative*, *negatively-small*, *negatively-large*, and *very-negative*.

$$f(c, \delta; x) = \begin{cases} \exp\left(\frac{-(x-c)^2}{2\delta^2}\right), & \text{if } x > c, \\ 1, & \text{if } x \leqslant c. \end{cases} \tag{15}$$

Next, the *linguistic values*, *large*, *positive*, *positively-small*, *positively-large*, and *very-positive*, are specified by (16).

$$g(c, \delta; x) = \begin{cases} 1, & \text{if } x > c, \\ \exp\left(\frac{-(x-c)^2}{2\delta^2}\right), & \text{if } x \leqslant c. \end{cases} \tag{16}$$

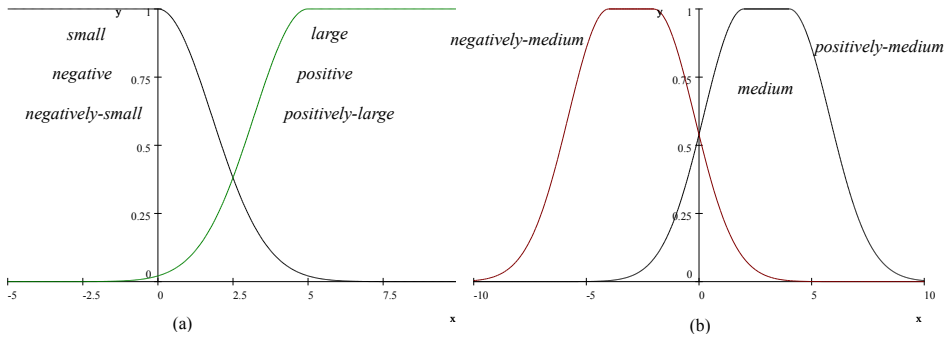

Fig. 4. Four membership functions. $f(c, \delta; x)$ where $c = 0$, $\delta = 1.8$. $g(c, \delta; x)$ where $c = 5$, $\delta = 1.8$. $z_1(c_1, \delta_1, c_2, \delta_2; x)$ where $c_1 = 2$, $\delta_1 = 1.8$, $c_2 = 4$, $\delta_2 = 1.8$. $z_2(c_1, \delta_1, c_2, \delta_2; x)$ where $c_1 = -2$, $\delta_1 = 1.8$, $c_2 = -4$, $\delta 2 = 1.8$.

In (16), these two parameters, c and δ, are the center and spread of a bell-shape function, respectively. Figure 4(a) displays two membership functions which are defined by (15) and (16), respectively. A linguistic hedge, "*very*", serves as a concentration for atomic terms. Therefore, the above membership functions for these two composite terms, *very-negative* and *very-positive*, can be rewritten as f^d and g^d, respectively, where $d > 1$. In this paper, d is set to 2. Subsequently, the membership functions for medium, *positively-medium*, and *negatively-medium* are defined by

$$z(c_1, \delta_1, c_2, \delta_2; x) = \begin{cases} \exp(\frac{-(x-c_1)^2}{2\delta^2}), & \text{if } x < c_1, \\ 1, & \text{if } c_1 \leqslant x \leqslant c_2, \\ \exp(\frac{-(x-c)^2}{2\delta^2}), & \text{if } x > c_2, \end{cases} \tag{17}$$

where c_1 and c_2 are positive for medium and *positively-medium*, but negative for *negatively-medium*. Figure 4(b) shows two membership functions defined by (17). A set Φ of parameters specifies the membership functions of all linguistic values in the FIS of the AIWJFG technique, which can be expressed as

$$\Phi = \left\{ \Phi_{rj} \;\middle|\; 1 \leqslant r \leqslant 14,\ 1 \leqslant j \leqslant 4,\ (r, j) \notin \{1, 2, \ldots, 6\} \times \{3\} \right\}.$$

If the jth linguistic term in the rth rule is defined by (15) or (16), then $\Phi_{rj} = (c_{rj}, \delta_{rj})$, if the jth linguistic term in the rth rule is defined by (17), then $\Phi_{rj} = (c_{rj,1}, \delta_{rj,1}, c_{rj,2}, \delta_{rj,2})$ where c_{rj} and δ_{rj} denote the center and spread of the membership function of the jth linguistic term in the rth fuzzy rule, respectively. Consequently, Φ is composed of 136 parameters. An example of $(r, j) = (1, 4)$, c_{14}, and δ_{14} stand for the center and spread of the membership function, respectively, for the linguistic term *very-positive* in the consequent part of the first fuzzy inference rule in Φ. For simplicity, the denotation $(c_{rj,1}, \delta_{rj,1}, c_{rj,2}, \delta_{rj,2})$ can be regarded as (c_{rj}, δ_{rj}) hereafter.

A set of parameter values for Φ decides the performance of the FIS. Therefore, in order for reducing the searching time while exploiting a GA as a method of searching a

near-optimal solution for Φ, a simple way is to specify appropriate ranges of the center and spread of each membership function. Consequently, the center c_{rj} and spread δ_{rj} for each (c_{rj}, δ_{rj}), which characterize the shape of its corresponding membership function, can be rewritten, respectively, as

$$c_{rj} = \mu^{\Psi(c_{rj},\delta_{rj})} + h\big(\Delta(c_{rj}, \delta_{rj})\big)c_{rj}^{\mu}\sigma^{\Psi(c_{rj},\delta_{rj})}, \tag{18}$$

and

$$\delta_{rj} = \delta_{rj}^{\sigma}\sigma^{\Psi(c_{rj},\delta_{rj})}, \tag{19}$$

where $\Psi(c_{rj}, \delta_{rj}) \in \{G, U, V\}$, $\Delta(c_{rj}, \delta_{rj}) \in \Delta = \Delta_{PO} \cup \Delta_{NE}$,

$$\begin{cases} \mu^a = \dfrac{1}{m \times n}\displaystyle\sum_{k=1}^{m\times n} a_{\rho_k}, \\ \sigma^a = \dfrac{1}{m \times n}\displaystyle\sum_{k=1}^{m\times n} \big(a_{\rho_k} - \mu^a\big)^2)^{\frac{1}{2}}, \quad a \in \{G, U, V\}, \end{cases} \tag{20}$$

$$h\big(\Delta(c_{rj}, \delta_{rj})\big) = \begin{cases} 1, & \text{if } \Delta(c_{rj}, \delta_{rj} \in \Delta_{PO}), \\ -1, & \text{if } \Delta(c_{rj}, \delta_{rj} \in \Delta_{NE}), \end{cases} \tag{21}$$

$$\Delta_{PO} = \left\{ \begin{array}{l} \textit{small},\ \textit{medium},\ \textit{large},\ \textit{positive},\ \textit{positively-small}, \\ \textit{positively-medium},\ \textit{positively-large},\ \textit{very-positive} \end{array} \right\}$$

and

$$\Delta_{NE} = \left\{ \begin{array}{l} \textit{negatively},\ \textit{negatively-small},\ \textit{negatively-medium}, \\ \textit{negatively-large}, \textit{very-negative} \end{array} \right\}.$$

Here $\Psi(c_{rj}, \delta_{rj})$ denotes a fuzzy variable in the jth atomic fuzzy proposition of the rth rule, which has a linguistic value $\Delta(c_{rj}, \delta_{rj})$ identified by (c_{rj}, δ_{rj}) in (18) and (19). Additionally, in (20), μ^a and σ^a represent the estimate sample mean and the estimate sample deviation of $\{a'_{\rho_k} \mid 1 \leqslant k \leqslant m \times n\}$, respectively, for $a \in \{G, U, V\}$. Subsequently, Φ can be rewritten as (22).

$$\Phi = \big\{\Phi_{rj} = \big(c_{rj}^{\mu}, \delta_{rj}^{\sigma}\big) \mid 1 \leqslant r \leqslant 14,\ 1 \leqslant j \leqslant 4,\ (r, j)\{1, 2, \ldots, 6\} \times \{3\}\big\}. \tag{22}$$

For instance, in the first rule in Table 2, $(c_{11}^{\mu}, \delta_{11}^{\sigma})$ characterizes the linguistic value $\Psi(c_{11}, \delta_{11})$, *small*, of the fuzzy variable $\Psi(c_{11}, \delta_{11})$, G.

Mamdani's method is applied to realize Fuzzy Inference Engine of the FIS in the AI-WJFG technique, while evaluating a fuzzy output of each fuzzy rule (Ross, 2004). Moreover, the aggregation method adopts the maximum operation to aggregate these 14 fuzzy

outputs. Furthermore, Defuzzifier is implemented with the centroid calculation. An advantage of the AIWJFG technique is to exploit the FIS in the watermark extraction without the information of original images. For an input $(G'_{\rho_k}, U'_{\rho_k}, V'_{\rho_k})$ corresponding to a watermarked image block X'_{ρ_k}, the $(G'_{\rho_k}, U'_{\rho_k}, V'_{\rho_k})$ is fed into the FIS, and then the FIS estimates $\hat{w}_k$ ranging from -1 to 1. The estimated watermark bit should be binary, therefore $\hat{w}_k$ is determined by

$$\hat{w}_k = \begin{cases} 0, & \hat{w}_k < T_{WE}, \\ 1, & \text{else}, \end{cases} \tag{23}$$

where T_{WE} denotes a threshold in $[-1, 1]$. In the experiment of the paper, the optimal threshold T_{WE} can also be decided by using a GA. Namely, Φ is updated as $\Phi \leftarrow \Phi \cup \{T_{WE}\}$. The cardinality of the set Φ is 137, that is, $|\Phi| = 137$.

3.6. *An FIS Optimized by a GA*

The watermark-extraction performance of the AIWJFG technique depends on a set of values for Φ. It is ineficient and time-consuming to search for an optimal solution for Φ while using the manual or the brute-force methods. Accordingly, the AIWJFG technique exploits a GA as a scheme of finding out a near-optimal solution for Φ systematically (Ross, 2004). Figure 5(a) illustrates the procedure of using a simple GA to search for a near-optimal solution, characterizing the FIS, for Φ. Let Φ^{P_j} denote the P_jth chromosome representing a set of near-optimal values. The structure of a chromosome, which represents a set of values for Φ, is displayed in Fig. 5(b). In this paper, each parameter in Φ is encoded by 8 bits, thus a chromosome has 1096 bits. In the implementation of the AIWJFG technique, Table 3 presents several control parameters, the length of a chromosome, the size of the population (the number of individuals), the number of the generation, crossover rate, mutation rate, and ranges for all parameters in Φ. Furthermore, in Fig. 5(a), the fitness function in Fitness computation component is performed using BCR which is specified in (25).

4. Experimental Results

A 64×64 stamp binary image, as shown in Fig. 6(a), is taken as the signature to identify the image copyrights in this experiment. Hence m and n are set to 64. By using a row-major algorithm, a binary image can be converted to a binary sequence with length 4096. Here the binary sequence represents the original watermark W. The performance of watermarking methods is investigated by measuring their imperceptibility and robustness. For the imperceptible ability, a quantitative index, Peek Signal-to-Noise Ratio (PSNR), is employed to evaluate the similarity between an original image X and a watermarked image X'. For the robust ability, Bit Correction Rate (BCR) measures the similarity between

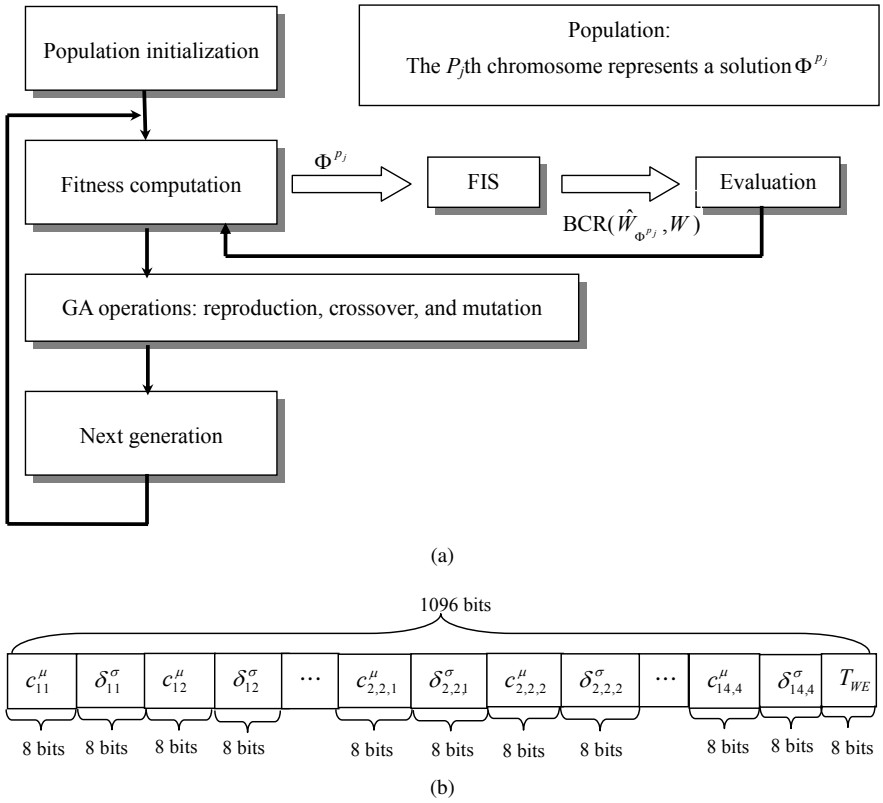

Fig. 5. (a) The procedure of using a GA to search a near-optimal solution for Φ characterizing the FIS. (b) A structure of a chromosome.

Table 3
Values for parameters used in the GA algorithm. If the linguistic terms are negative or very negative, the center c_{rj}^{μ} of their associated membership functions is in $[-2, -1]$ or vice versa.

The linguistic terms	Parameters
Length of a chromosome	1096 (bits)
Number of individuals (population size)	100
Maximum number of generations	50
Crossover rate	0.8
Mutation rate	0.05
Ranges of c_{rj}^{μ} and δ_{rj}^{σ}, for $1 \leqslant r \leqslant 6$, $1 \leqslant j \leqslant 2$	[0.01, 1.29]
Ranges of c_{rj}^{μ} and δ_{rj}^{σ}, for $7 \leqslant r \leqslant 14$, $1 \leqslant j \leqslant 3$	[0.01, 1.29]
Ranges of c_{rj}^{μ}, for $1 \leqslant r \leqslant 14$, $j = 4$	$[-2, -1]$ or $[1, 2]$
Ranges of δ_{rj}^{σ}, for $1 \leqslant r \leqslant 14$, $j = 4$	[0.01, 1.29]
Range of the threshold TWE	$[-1, 1]$

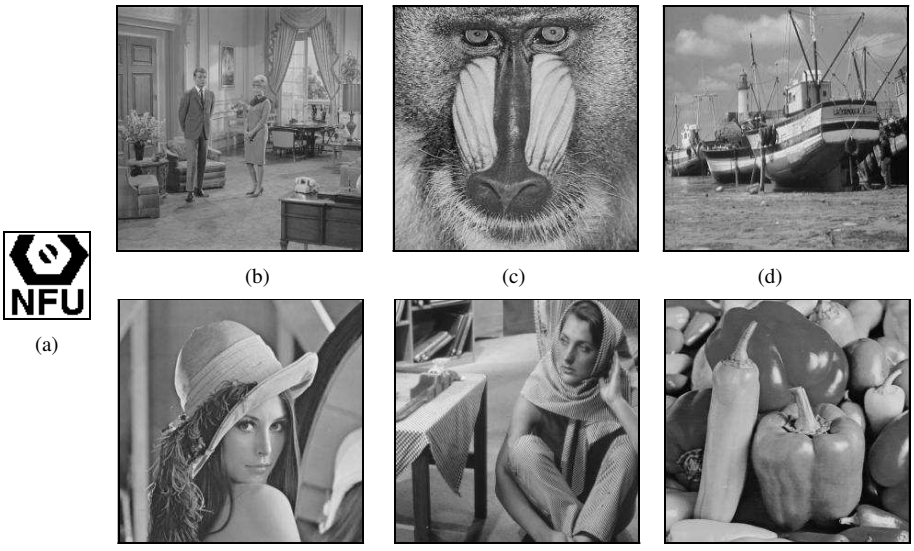

Fig. 6. (a) The original watermark. (b–g) are the watermarked images, Couple, Baboon, Boat, Lena, Barbara, and Pepper, respectively.

an original watermark W and the extracted watermark $\hat{W}$. The PSNR and the BCR are, respectively, defined by

$$\mathrm{PSNR}(X, X') = 10\log_{10} \frac{255 \times 255}{\frac{\sum_{i=0}^{M-1}\sum_{j=0}^{N-1}(x_{ij}-\bar{x}_{ij})^2}{M\times N}} \tag{24}$$

and

$$\mathrm{BCR}(W, \hat{W}) = 1 - \frac{\sum_{k=1}^{m\times n}|w_k - \hat{w}_k|}{m \times n}. \tag{25}$$

Higher PSNR indicates the original image X more resembles the watermarked image X'. The result that a watermarking method has high PSNR reveals that it makes watermarks more imperceptible. Higher BCR conveys that an original watermark W is more similar to the extracted watermark $\hat{W}$. A watermarking method performs a high robustness if it gets a low BCR while retrieving the watermark from an attacked (degraded) image. In the experiment of the paper, the watermarked image X' can be further degraded by intentional and unintentional operations.

Six images with size 512×512 are examined in the experiment. Therefore, M and N equal 512. After embedding Fig. 6(a) in the original versions of these six images, their watermarked images, Couple, Baboon, Boat, Lena, Barbara, and Peppers, are displayed in Figs. 6(b)–6(h), respectively. Let X^j and X'^j denote the original and watermarked images, respectively, where $j \in \{\text{Couple, Baboon, Boat, Lena, Barbara, Peppers}\}$. Table 4 exhibits the comparison results in terms of the average of PSNRs for six watermarked

Table 4
Comparison results in terms of the average of PSNRs for the six watermarked images produced by four methods.

Method	AIWJFG	Joo	Moon	Wang
The average PSNRs	40.82	31.11	35.40	37.47

images, X'^{j}, for all j. Observing Figs. 6(b)–6(h), it is hard to discern visible distortions on them. Consequently, the results demonstrate that the AIWJFG technique definitively makes watermarks quite imperceptible.

4.1. *Attack-Free Case*

In the attack-free case, a watermarked image X'^{j} and the watermark W in Fig. 6 are employed to search a near-optimal set $\Phi^{o,j}$ for Φ. Note that the searching process for Φ is called a training process of the FIS. Let $\Omega_j = \{(X'^{j}_{\rho k}, w_k) \mid k = 1, 2, \ldots, 4096\}$ denote a set of training patterns constructed by $\{X'^{j}, W\}$ where $X'^{j}_{\rho k}$ and w_k are called an input vector and its corresponding desired output, respectively. More specifically, a near-optimal set $\Phi^{o,j}$ can be found after presenting a GA with Ω_j. For a watermarked image X'^{j}, let Φ'^{j} and $\Phi^{o,j}$ represent a set of values for a chromosome in the initial population and a set of near-optimal values for the best chromosome among the final population, respectively. When Φ'^{j} and $\Phi^{o,j}$ are separately applied to identify the fuzzy rules in the FISs of the AIWJFG technique, Φ'^{j} characterizes an initial FIS (before training), but $\Phi^{o,j}$ characterizes the trained FIS (after training). Subsequently, a set $\{X'^{j}_{\rho k} \mid k = 1, 2, \ldots, 4096\}$ of testing patterns is fed into the AIWJFG technique and then to yield an estimated watermark $\hat{W}^{o,j}$. In the attack-free case, input vectors $X'^{j}_{\rho k}$ of training patterns in Ω_j are the same as the testing patterns $X'^{j}_{\rho k}$. Therefore, the process can be viewed as an evaluation for the memorized capability of the AIWJFG technique. Figure 7 shows the comparison results in terms of the averages of the BCR values for the six images. Additionally, Fig. 8 exhibits the visual comparison results for estimated watermarks which are retrieved by using the AIWJFG technique and other existing methods being considered here (Joo *et al.*, 2002; Moon *et al.*, 2007; Wang and Pearmain, 2004). Obviously, the AIWJFG technique is superior to existing methods in the attack-free case.

4.2. *Robustness Investigation*

In the process of investigating the robustness of the AIWJFG technique, several common image manipulations, including brighten, darken, cropping, painting, noising, histogram equalization, sharpening, blurring, and JPEG2000 compression/ decompression, are simulated as attacks to degrade watermarked images. Let $X'^{j,\tau}$ denote an attacked-and-watermarked image which is obtained by further manipulating X'^{j} while using an attack $\tau \in \{$brightening, darkening, cropping, painting, noising, histogram equalization, sharpening, blurring, and JPEG2000 compression/ decompression, stirmark$\}$. Figure 9 displays some attacked-and-watermarked images selected from $\{X'^{j,\tau} \mid$ for all $j\}$, a set of attacked-and-watermarked images.

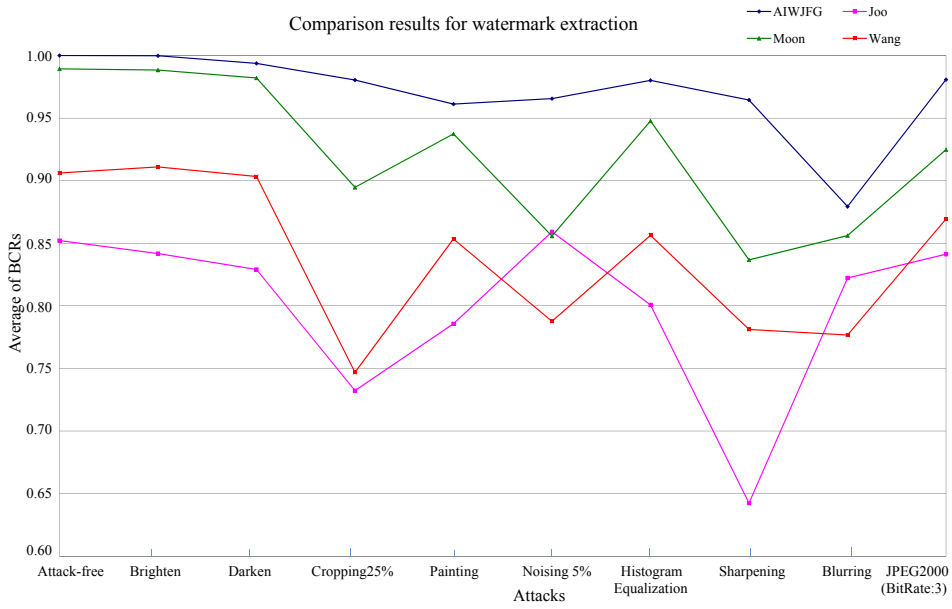

Fig. 7. Comparison results in terms of the average of BCRs for six examined images for robustness test.

	Couple	Baboon	Boat	Lena	Babara	Pepper
AIWJFG						
Joo						
Moon						
Wang						

Fig. 8. In the attack-free case, estimated watermarks are extracted by using the AIWJFG technique, Joo's, Moon's, and Wang's methods for six examined images.

In the robustness-investigation phase, the parameter set $\Phi^{o,j}$, characterizing the AIWJFG technique, is the same as that exploited in the attack-free case. Subsequently, a set $\{X'^{j,\tau}_{\rho k} \mid k = 1, 2, \ldots, 4096\}$ of testing patterns, which differs from $\{X'^{j}_{\rho k} \mid k = 1, 2, \ldots, 4096\}$, is fed into the AIWJFG technique to produce an estimated watermark $\hat{W}^{o,j}$. Here the set of input vectors of training patterns in Ω_j, which is constructed from (X'^{j}, W), differs from the set of testing patterns. The investigation can be treated as the robustness evaluation to endure attacks. Computer simulations of these attacks mentioned above are briefly described as follows.

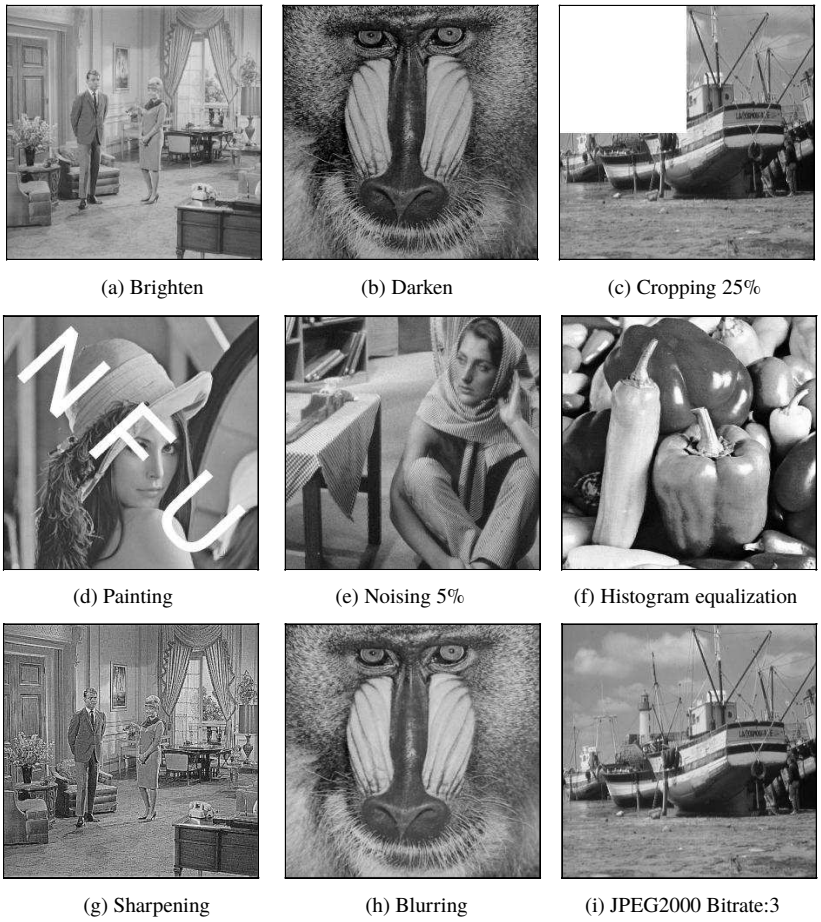

(a) Brighten (b) Darken (c) Cropping 25%

(d) Painting (e) Noising 5% (f) Histogram equalization

(g) Sharpening (h) Blurring (i) JPEG2000 Bitrate:3

Fig. 9. The manipulated-and-watermarked images for attacks simulated by nine image manipulations.

- Brightening: the brighten attack is performed by adding a positive constant to the pixels of the entire watermarked image X'^{j}. Figure 9(a) exhibits an example $X'^{j,brightening}$ for $j =$ "Couple".
- Darkening: the dark attack is simulated by subtracting a positive constant from the pixels of the whole watermarked image. Figure 9(b) shows an example $X'^{j,darkening}$ for $j =$ "Baboon".
- Cropping: the cropping attack is carried out by cropping the upper-left region with size 256×256 from X'^{j}. Figure 9(c) displays an example $X'^{j,cropping}$ for $j =$ "Boat". This is called pseudo-cropping due to still keeping the original spatial reference to the upper-left pixel. A formal cropping consists in selecting a (possibly) random part of an image and then creating another one by discarding the parts that were not selected. In the case, the simulation just blanks out a part of a watermarked image.

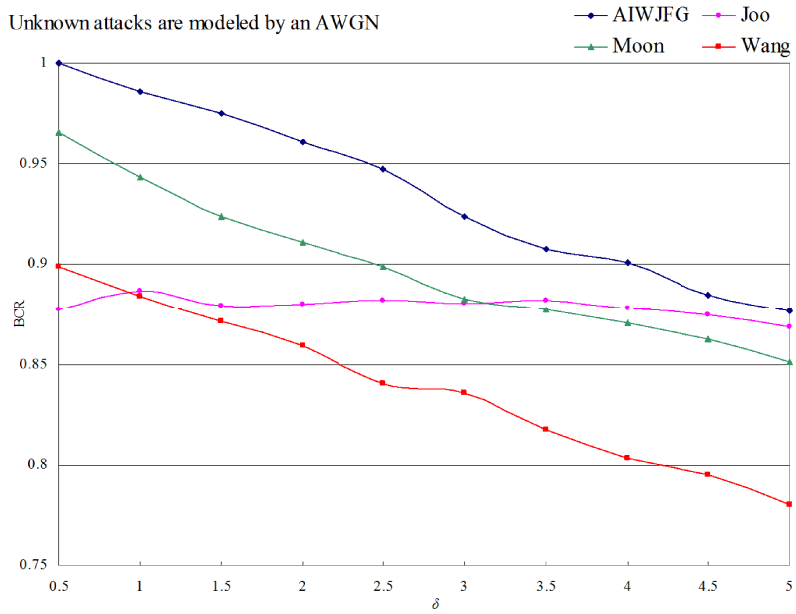

Fig. 10. A comparison result for robustness assessment for unknown exact attacks via using a way Gaussianity models the uncertainty of the attacks.

- Painting: We paint "NFU" on X'^{j} and then get $X'^{j,painting}$. Figure 9(d) exhibits an example $X'^{j,painting}$ for $j =$ "Lena".
- Noising: a noising scheme is performed by generating impulsive noises (Own *et al.*, 2006). The corrupted-and-watermarked image $X'^{j,noising,l\%}$ is obtained by adding $l\%$ impulsive noises in a watermarked image X'^{j}. An example $X'^{j,noising,5\%}$ is displayed in Fig. 9(e) for $j =$ "Barbara". Because the exact attack to be undergone is unknown, there is a way the watermarking community nowadays assesses robustness. It is modeled by an AWGN (Additive White Gaussian Noise) addition to the image. Gaussianity models the uncertainty of the attack. Variance of the noise models the severity of the attack. Let an AWGN follow $N(0, \delta 2)$. Figure 10 shows a comparison result plotting the BCR w.r.t. the noise power δ.
- Histogram equalization: the purpose of the histogram-equalization scheme is to gain a new enhanced image with an uniform histogram. The degraded-and-watermarked image $X'^{j,histogram\ equalization}$ is produced by applying the histogram-equalization scheme to X'^{j}. An example x'^{j} is shown in Fig. 9(f) for $j =$ "Peppers".
- Sharpening: the sharpen attack is performed by using a 3×3 spatial sharpen filter for a watermarked block X'_{ij}. The output of the filter can expressed as the form

$$x'_{ij} = 10x'_{ij} - \sum_{k=-1}^{1} \sum_{l=-1}^{1} x'_{i+k,j+l} \tag{26}$$

where x'_{ij} stands for the center pixel x'_{ij} in X'_{ij}. An example $X'^{j,sharpening}$ is exhibited in Fig. 9(g) for $j =$ "Couple".

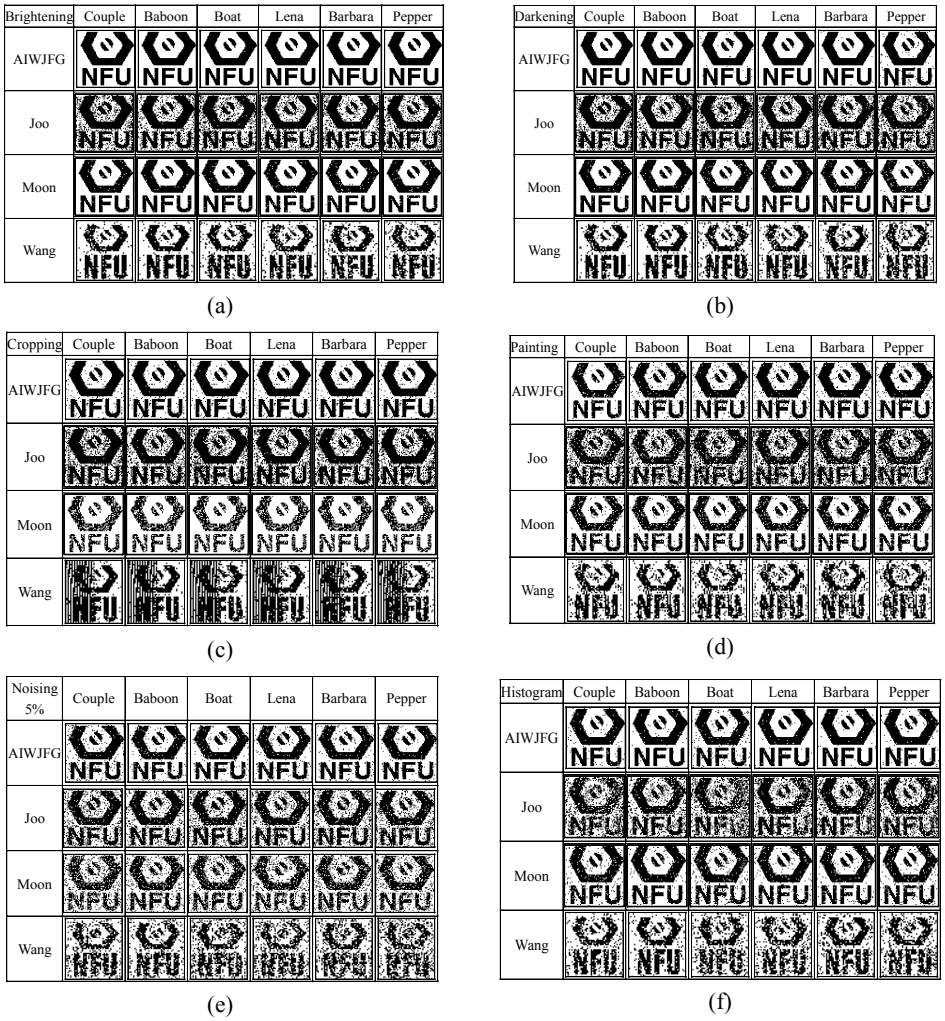

Fig. 11. The comparison results for the robustness of the AIWJFG technique, Joo's, Moon's, and Wang's methods for (a) Brighten, (b) Darken, (c) Cropping, (d) Painting, (e) Noising, (e) Histogram, (g) Sharpening, (h) Blurring, and (i) JPEG2000 attacks.

- Blurring: the blurring operation for the center pixel x'_{ij} in a watermarked block X'_{ij} is implemented by

$$x'_{ij} = \frac{1}{16}\left[\left(\sum_{k=-1}^{1}\sum_{l=-1}^{1} x'_{i+k,j+l}\right) + 7x'_{ij})\right]. \tag{27}$$

  Figure 9(h) shows an example $X'^{j,blurring}$ for $j =$ "Baboon".
- JPEG 2000 compression/decompression: a degraded-and-watermarked image $X'^{j,JPEG2000,l}$ is produced by first compressing x'_{ij} with JPEG2000 compression at

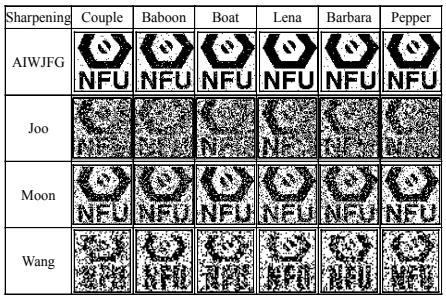

(g)

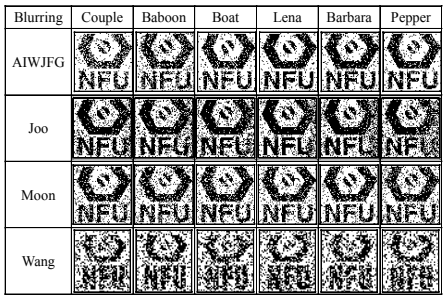

(h)

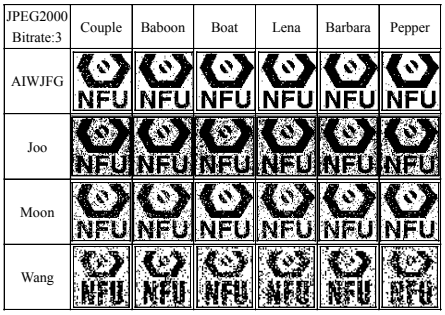

(i)

Fig. 11. *Continued.*

bitrate l and then by decompressing the compressed version of X'^j. Because JPEG compression is a lossy compression method, the visual quality of $X'^{j,JPEG2000,l}$ depends on the bitrate l. $X'^{j,JPEG2000,l}$ has more poor visual quality if X'^j is compressed at lower bitrate l. Here JPEG2000 compression/decompression is simulated by exploiting the Ulead PhotoImpact software. Figure 9(i) displays an example $X'^{j,JPEG2000,l}$ for $j =$ "Boat" and $l = 3$.

- Stirmark: the stirmark benchmark is also exploited in robustness evaluation and it is available at Stirmark (2008). Three attacks, psnr, noise, and jpeg, are involved in the test, and 10 levels are produced for each attack. The ranges of psnr, noise, and jpeg are [10, 100], [0.5, 5], and [10, 100], respectively. Figure 7 exhibits the comparison results, which are represented by the average of BCR values for 30 cases for the three attacks.

Observing Fig. 7, the AIWJFG technique cannot perform very well in blurring and Stirmark attacks in contrast to others cases. In the case of the blurring attack, the blurring operation in (27) damages image details and edges. It leads to seriously destroy the watermarks being embedded in the image details and edges while employing (5) and (7) for the watermark extraction. Regarding to the case of the Stirmark benchmark, it carries out a combination of three image-processing manipulations which are developed in spatial and frequency domains. Therefore, the kind of attacks can seriously destroy image features. Observing Fig. 11, the AIWJFG technique is also superior to the compared

methods under consideration here for a generic attack called the uncorrelated-noise attack which is simulated using an AWGN addition model. Additionally, Fig. 11 exhibits visual-perception results in terms of estimated watermarks for comparing the robustness of the AIWJFG technique with that of existing methods under consideration. From the above results, the AIWJFG technique indeed possesses satisfying imperceptible and robust capabilities for withstanding the common attacks under consideration. Meanwhile, it also remarkably outperforms other proposed methods being considered here.

5. Conclusions

This paper has proposed a novel watermarking technique, the AIWJFG technique, based on the JND profile of images and techniques of FISs and GAs. During watermark embedding, the AIWJFG technique embeds a watermark into an image by referring the JND profile of an image so that it makes the watermark further imperceptible. The AIWJFG technique employs image features and local statistics of the watermarked image while creating an FIS. During watermark extraction, the AIWJFG technique utilizes the FIS to extract watermarks without original images. The FIS can be further optimized (trained) by a GA so that its watermark-extraction performance can be improved effectively. Experimental results are provided to prove that the AIWJFG technique not only makes watermarks further imperceptible but also possesses adaptive and robust capabilities against the image-manipulation attacks under consideration. Consequently, the results demonstrate that the AIWJFG techniques can serve as an approach of protecting image copyrights from being counterfeited.

Acknowledgments. Authors would like to thank the National Science Council of Taiwan, R.O.C., for financially supporting this research under Contract Nos. NSC 97-2221-E-150-070 and NSC 99-2511-S-150-002. Our gratitude is extended to the anonymous reviewers for their valuable comments and professional contributions to the improvement of this paper.

References

Arakawa, K. (1996). Median filters based on fuzzy rules and its application to image processing. *Fuzzy Sets and Systems*, 77, 3–13.

Blum, L., Blum, M., Shub, M. (1986). A simple unpredictable pseudo-random number generator. *SIAM Journal on Computing*, 15(2), 364–383.

Barni, M., Bartolini, F., Piva, A. (2001). Improved wavelet-based watermarking through pixel-wise masking. *IEEE Transactions on Image Processing*, 10(5), 783–791.

Chou, C.H., Li, Y.C. (1995). A perceptually tuned subband image coder based on the measure of just-noticeable-distortion profile. *IEEE Transactions on Circuits and Systems for Video Technology*, 5(6), 467–476.

Chang, C.-H., Ye, Z., Zhang, M. (2005). Fuzzy-ART based adaptive digital watermarking scheme. *IEEE Transactions on Circuits and Systems for Video Technology*, 15(1), 65–81.

Delaigle, J.F., De Vleeschouwer, C., Macq, B. (1998). Watermarking algorithm based on a human visual model. *Signal Processing*, 66, 319–335.

Hsu, C.T., Wu, J.L. (1999). Hidden digital watermarks in images. *IEEE Transactions on Image Processing*, 8, 58–68.

Hsieh, M.-S., Tseng, D.-C. (2005). Multiresolution image watermarking using fuzzy inference filter. In: *Proceeding of Computational Intelligence*, p. 487.

Jain, A.K. (1989). *Fundamentals of Digital Image Processing*. Prentice Hall, Upper Saddle River.

Joo, S., Suh, Y., Shin, J., Kikuchi, H., Cho, S.-J. (2002). A new robust watermark embedding into wavelet DC components. *ETRI Journal*, 24, 401–404.

Lou, D.-C., Yin, T.-L. (2002). Adaptive digital watermarking using fuzzy logic techniques. *Optical Engineering*, 41, 2675–2687.

Mukherjee, D.P., Maitra, S.S., Acton, T. (2004). Spatial domain digital watermarking of multimedia objects for buyer authentication. *IEEE Transactions on Multimedia*, 6(1), 1–15.

Moon, H.S., You, T., Sohn, M.H., Kim, H.S., Jang, D.S. (2007). Expert system for low frequency adaptive image watermarking: Using psychological experiments on human image perception. *Expert Systems with Applications*, 32(2), 674–686.

Own, C.-M., Tsai, H.-H., Yu, P.-T., Lee, Y.-J. (2006). On the design of adaptive type-2 fuzzy median filter for removal of impulsive noises. *Imaging Science Journal*, 54(1), 3–16.

Paquet, A.H., Ward, R.K., Pitas, I. (2003). Wavelet packets-based digital watermarking for image verification and authentication. *Signal Processing*, 83, 2117–2132.

Ross, T.J. (2004). *Fuzzy Logic with Engineering Applications*, 2th ed. Wiley, Hoboken.

Shih, F.Y., Wu, S.Y.T., (2003). Combinational image watermarking in the spatial and frequency domains. *Pattern Recognition*, 6, 969–975.

Stirmark Benchmark (2008). http://www.petitcolas.net/fabien/watermarking/stirmark/ (retrieved 12.05.08).

Tsai, H.-H., Liu, C.-C. (2011). Wavelet-based image watermarking with visibility range estimation based on HVS and neural networks. *Pattern Recognition*, 44(4), 751–763.

Tsai, H.-H., Sun, D.-W. (2007). Color image watermark extraction based on support vector machines. *Information Sciences*, 177, 550–569.

Tsai, H.-H., Wang, K.-C. (2008). Wavelet-domain image watermarking based on rank order and classiffcation approach optimized by genetic algorithm. *Imaging Science Journal*, 56(16), 201–216.

Umbaugh, S.E. (1998). *Computer Vision and Image Processing: A Practical Approach Using CVIP Tools*. Prentice Hall, Upper Saddle River.

Wang, L.X. (1997). *A Course in Fuzzy Systems and Control*. Prentice Hall, Upper Saddle River.

Wang, Y., Pearmain, A. (2004). Blind image data hiding based on self reference. *Pattern Recognition Letters*, 25, 1681–1689.

Yu, P.-T., Tsai, H.-H., Lin, J.-S. (2001). Digital watermarking based on neural networks for color images. *Signal Processing*, 81(3), 663–671.

Yu, G.-J., Lu, C.-S., Liao, H.-Y.M. (2003). A message-based cocktail watermarking system. *Pattern Recognition*, 36, 957–968.

Zhao, Y., Campisi, P., Kundur, D. (2004). Dual domain watermarking for authentication and compression of cultural heritage images. *IEEE Transactions on Image Processing*, 13(3), 430–448.

H.-H. Tsai received the BS and the MS degrees in applied mathematics from National Chung Hsing University, Taichung, Taiwan, in 1986 and 1988, respectively, and the PhD degree in computer science and information engineering from National Chung Cheng University, Chiayi, Taiwan, in 1999. Currently, he is a professor at Department of Information Management, National Formosa University, Huwei, Yulin, Taiwan. He has worked in industry for the SYSTEX Corporation, and in academia for Nanhua University, Chiayi, Taiwan. He is an honorary member of the Phi Tau Phi Scholastic Honor Society. He has been selected and included in the 9th edition of Who's Who in Science and Engineering which has been published in 2006. He serves as a technical reviewer for various scientific journals and numerous international conferences. His research interests include computational intelligence, machine learning, support vector machines, multimedia security, digital watermarking, intelligent filter design, content-based multimedia retrieval, data mining, e-Learning and system integration with web services.

S.-C. Lo received the BS degree in mathematics from the National Taiwan University, Taipei, Taiwan, the MS degree in computer science and information engineering from the National Chung Cheng University, Chiayi, Taiwan, and the PhD degree in industrial and systems engineering from the University of Southern California, Los Angeles, California, USA. Since 2004, he has been with the Department of Industrial Management at the National Taiwan University of Science and Technology, Taipei, Taiwan, where he is currently an Assistant Professor. His research interests include fuzzy systems, operations research, intelligent transportation systems, logistics management, supply chain management, and information technology.

Vaizdo vandenženklių įterpimas ir ištraukimas, grindžiamas genetiniais algoritmais, grįstais neraiškiąja logika vaizdams verifikuoti

Hung-Hsu TSAI, Shih-Che LO

Šiame straipsnyje yra pristatoma prisitaikanti vaizdų vandenženklos technika, grindžiama nedidelių iškraipymų profilio analize ir neraiškiosios logikos išvadomis, apdorotomis genetiniu algoritmu. Vandens ženklo įterpimas atliekamas atsižvelgiant į vaizdo iškraipymų profilį. Profilį nusako lokalių vaizdo regionų statistikos, kiti vaizdo objektų požymiai, kurių pagrindu yra konstruojama neraiškiosios logikos sistema. Papildomai sistema yra optimizuojama genetinių algoritmų pagalba, kas leidžia iš esmės pagerinti vandens ženklo išskyrimo kokybę. Eksperimentų rezultatai rodo, kad pristatoma technika užtikrina, jog vandens ženklas nebus vizualiai matomas, be to yra atsparus vaizdo apdorojimo atakoms.